PAPER H

CROSSWELL TRAVELTIME TOMOGRAPHY USING DIRECT AND REFLECTED ARRIVALS: PART 2: EXAMPLES

Mark A. Van Schaack

ABSTRACT

The predicted resolution of reflector depth for an inversion of crosswell seismic data using direct and reflected traveling data is *several inches*. This prediction is for a survey with an acquisition geometry similar to the ~180 ft McElroy data set. The predicted reflector resolution for an inversion of data collected in a ~600 ft survey is 0.5-2.5 ft. I have run combined direct and reflected arrival traveltime tomography on 3 synthetic surveys and 1 field data survey and have obtained results very near to these theoretical predictions.

Resolution of reflector depths is very high in the crosswell traveltime inversion while velocity resolution remains mediocre. The extent to which reflector depths can be recovered suggests that direct and reflected arrival tomography may be an ideal tool for obtaining a velocity model and reflector geometries suitable for accurately mapping crosswell reflection data.

INTRODUCTION

In my first paper, Crosswell Traveltime Tomography using Direct and Reflected Arrivals—Part 1: Theory and Implementation, I presented an approach for using direct and reflected arrival traveltimes to solve for a 2-D slowness field and reflector depths simultaneously. While the potential of surface seismic reflection tomography has been heavily studied in the recent past, (Bishop et al., 1985; Ivansson, 1986; Stork, 1988; Bube et al., 1989) little work has been done in the area of crosswell reflection tomography. Partly this is because it has been only recently that reflections have been successfully extracted from crosswell data (Lazaratos, 1993; Lazaratos et al., 1995).

Calnan and Schuster (1989) compared direct arrival and combined direct and reflected arrival tomography in a theoretical study. This study was performed using straight rays, horizontal reflectors, and vertical boreholes. The conclusion of this study was that the primary benefit of direct and reflected arrival tomography was that it could yield a finer velocity resolution than allowed by direct arrival tomography.

More recently, resolution analyses were performed by Bube and Langan (1995) using acquisition parameters based on the 1991 and 1993 McElroy Reservoir Geosciences Project experiments (Harris et al., 1995). The motivation of these analyses was to obtain information on how well reflector depths and velocity might be resolved in a combined direct and reflected arrival inversion. Two synthetic problems were formulated: one based on the ~180 ft McElroy profile, and the other based on the ~600 ft profile. An extraordinary

result of these studies was that estimated errors in reflector depths were only a *few inches* for the 180 ft survey and 0.5–2.5 ft for the 600 ft survey. Another observation, consistent with those made in surface seismic tomography, was that good resolution of reflector depths could be expected in spite of mediocre velocity resolution.

In this paper I present the results of several combined direct and reflected arrival inversions. I primarily focus on the ability of these inversions to recover reflector depths accurately in these studies. Two of my synthetic studies are designed to test the ability of my program to handle nonlinear reflectors and discontinuous reflectors. In the last study I invert an *S*-wave direct and reflected arrival traveltime data set collected from the McElroy 188 ft offset profile. To aid the analysis of the field inversion I have created a synthetic data set using many of the field experiment's parameters and a velocity model with a structure similar to the field geology. I invert this data set using identical parameters as the field data set inversion.

FORWARD MODELING OF SYNTHETIC DATA SETS

The synthetic data sets found in this paper were all calculated using an eikonal-based forward modeling program that I have developed. This modeler uses a derivation of the finite-difference scheme introduced by Mo (1994). There are several advantages to using this approach to create synthetic crosswell reflection data sets. One advantage is that no raytracing or raypaths are required, making it very fast. Another advantage is that reflection traveltimes can be calculated very easily for arbitrary reflection surfaces. Another useful feature, related to the studies contained in this paper, is that this forward modeling program is different from the raytracer used in the tomography program. Other than both programs being based on ray theory, their approaches to calculating traveltimes are quite different. This should provide a better test of the effectiveness of the direct and reflected arrival tomography code.

Calculating Direct Arrival Traveltimes

Calculating direct arrival traveltimes is accomplished in one step using the finite-difference eikonal code. For each receiver location, a traveltime map is generated (I prefer "shooting" from receiver to source). Receiver to source traveltimes are read from the traveltime map location which coincides with the source. Bilinear interpolation is used when the source location does not reside on a grid node. The traveltimes are recorded for all source locations after which the code increments to the next receiver location. All receivers are "shot" in turn until the entire direct arrival traveltime data set has been acquired

Calculating Reflected Arrival Traveltimes

The first step in calculating reflection traveltimes is to compute traveltime maps for the source and receiver of interest. These source and receiver maps are then added together to create a single traveltime map. A fundamental characteristic of the combined map is that the traveltime stored at each node is the total traveltime from the source, to the node, and to the receiver. Once the combined traveltime map has been obtained, reflection traveltimes can be extracted from it.

The next step is to interpolate the reflector locations within the image area at a fine interval. Reflectors are defined by their depths recorded at several points across the image. The location of the reflector between these defined points is determined using a cubic spline interpolation method. This method is identical to that used in the raytracer described in my previous paper. It is necessary to interpolate the reflector position since it may be defined with as few as two points. The interpolation is usually done at the same interval as the image's node spacing in the x direction.

Once the reflector coordinates are defined, traveltimes are interpolated from the combined traveltime map for each of the points along the reflector. The reflection traveltime from source, to that reflector, and to the receiver, is simply the minimum traveltime along the reflector. Potentially the reflection point does not occur within the bounds of the image if the minimum traveltime is found at a reflector endpoint. When this occurs I record a null value for the source-receiver-reflector combination.

Reflection traveltimes can be found for any number of reflectors for the source-receiver combination used to create the combined traveltime map. To minimize computations I calculate reflection traveltimes for all reflectors before calculating a traveltime map for the next source-receiver pair. A NOTE ON EFFICIENCY: If sufficient computer memory exists traveltime maps for all source and receiver locations can be calculated beforehand. From this collection of maps a combined map can be created for any source-receiver combination simply by adding the appropriate source and receiver maps.

SYNTHETIC STUDY #1

The primary goal of the first synthetic study is to test the ability of direct and reflected arrival tomography to recover the geometries of straight and curved reflectors. I have created a simple model, shown in Figure 1, consisting of 3 layers and 4 reflectors. The layers are constant velocity although a mild 2-D filter has been run over the model to smooth the interfaces slightly.

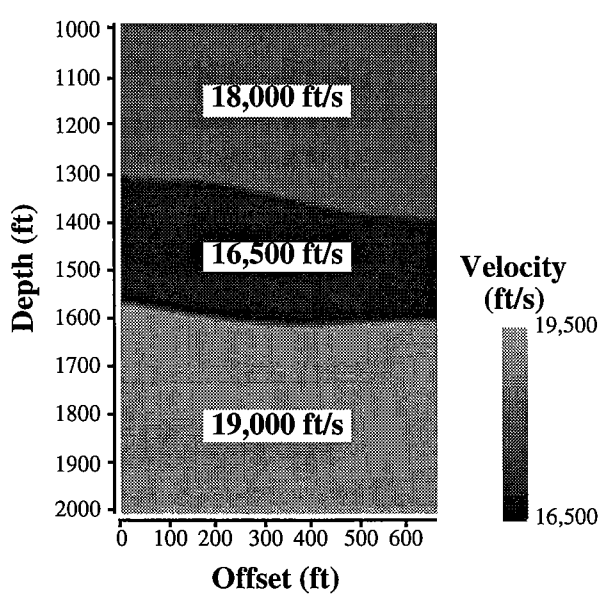

Figure 1: This figure shows the velocity distribution of model #1. The reflectors are defined by a cubic spline curve calculated from 8 evenly spaced points across the model.

The reflector definitions are shown in Table 1. As previously mentioned, the forward modeler interpolates between the defined reflector points using a cubic spline. In this example the top and bottom reflectors are linear and horizontal and reflectors 2 & 3 are curved, seen graphically in Fig. 1.

TABLE 1. Synthetic model #1 reflectors

Offset (ft)	0.0	94.29	188.57	282.86	377.14	471.43	565.71	660.0
Reflector 1	1003.0	1003.0	1003.0	1003.0	1003.0	1003.0	1003.0	1003.0
Reflector 2	1302.0	1310.0	1315.0	1335.0	1355.0	1375.0	1385.0	1392.0
Reflector 3	1569.0	1584.0	1600.0	1610.0	1615.0	1610.0	1607.0	1604.0
Reflector 4	1998.0	1998.0	1998.0	1998.0	1998.0	1998.0	1998.0	1998.0

Synthetic Study #1: Acquisition Geometry and Data Specifications

The synthetic survey is designed with 201 sources and 201 receivers spaced every 5.0 ft along the sides of the model shown in Fig. 1. The range of the sources and receivers is from 1000.0–2000.0 ft and the distance between the source and receiver wells is 660.0 ft. Direct and reflected arrival traveltimes were initially calculated for all source-receiver-reflector combinations in the forward modeling. In order to create a data set more closely resembling one that might come from the field, I edited these traveltimes by setting unlikely combinations to zero.

To prepare the direct arrival data set I zeroed traveltimes for source-receiver pairs at near and far offsets. Near offset traveltimes are often thought to be unreliable in field data sets due to head waves. For this test I muted traveltimes if the source and receiver were within 75 ft of each other in depth, approximately ±6.5° about the horizontal. I also muted traveltimes with a source/receiver offset greater than ~940 ft, ±55.0°, in part to reduce the size of the inversion problem, and in part because far offset traveltimes can be difficult to pick.

There are several observations which I have used to edit the synthetic reflected arrival traveltimes. One is that reflections are most visible in processed ~600 ft offset surveys for angles of incidence ranging from approximately 40-65° (Lazaratos, 1993; Lazaratos, personal comm.). Another observation is that it is difficult to pick traveltimes of a single reflector for both up and downgoing reflections reliably. I edited reflection traveltimes on the basis of upgoing or downgoing, and for a range of Common Depth Point (CDP) elevations chosen to keep the incidence angles of the rays approximately 40-65°. In crosswell experiments the CDP elevation of a source/receiver pair is

$$\mathbf{CDP}_{\mathrm{elev}} = \frac{\mathbf{ELEV}_{\mathrm{rec}} + \mathbf{ELEV}_{\mathrm{sou}}}{2.0} \tag{1}$$

In Table 2 I indicate the edited non-zero reflected arrival traveltimes based on the direction of the reflection and the CDP range.

TABLE 2. Specifications of Example 1 reflection traveltime data

	Direction	CDP Range (ft)	# Traveltimes
Reflector 1	downgoing	1187.0–1390.0	6887
Reflector 2	downgoing	1500.0–1702.0	6456
Reflector 3	upgoing	1217.0–1421.0	6239
Reflector 4	upgoing	1609.0–1812.0	6501

Synthetic Study #1: Inversion and Results

I ran a direct and reflected arrival inversion on the synthetic data set starting with a homogeneous slowness model and flat reflectors defined by 8 nodes at 1000.0, 1347.0 1586.0, and 2000.0 ft. I set the initial horizontal smoothing penalty weight equal to the traveltime data weight and the vertical smoothing penalty to1/4th of the horizontal value. The initial value of the reflector second derivative smoothing penalty weight was 1/100th the horizontal weight at the beginning of the inversion. The horizontal and vertical smoothing penalty terms were relaxed an order of magnitude every 4 continuation steps and the reflector penalty term was relaxed an order of magnitude every 2 continuation steps.

The ideal, or "best", answer of this inversion is the result of continuation step 12. By this step the horizontal penalty term, the strongest of the three, has only 4% of the weight of the traveltime data. Traveltime residuals are ~58μs root-mean-square (rms) for the 24,327 reflected rays and ~28μs rms for the 33,993 direct arrival rays. Figure 2 shows the results of the velocity tomogram.The velocity tomogram recovers the homogeneous nature of the 3 zones reasonably well. The curved nature of the interfaces bounding the low velocity central layer is also seen in the tomogram although the interfaces themselves are a somewhat blurred.

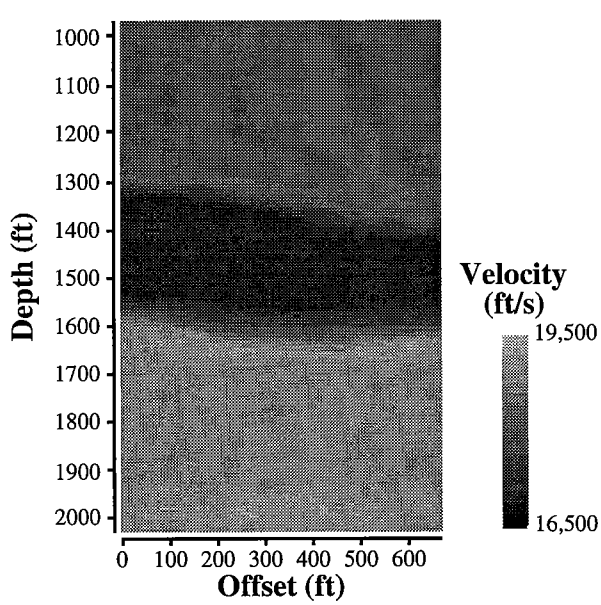

Figure 2: The velocity tomogram resulting from 12 continuation steps of a combined direct and reflected arrival traveltime inversion. Compare this result with the original velocity model used to create the synthetic data seen in Fig. 1.

The recovered reflector parameters, shown inTable 3, have distinctly higher resolution. Unfortunately, a direct comparison cannot be made between the parameters seen in Table 3 and those listed in Table 1. In spite of the fact that 8 parameters are used for each reflector description there is a slight difference in the offsets in the two parameter sets which can be noted across the top of each table. The difference is because the tomogram is 670.0 ft across while the source-receiver offset is 660.0 ft. The raytracer used in the inversion program requires the sources (on the right side of the model) to lie *within* the model so an extra pixel was added to the right of the model for the inversion.

TABLE 3. Example 1 reflector depth inversion results

Offset (ft)	0.0	95.7	191.4	287.1	382.8	478.6	574.3	670.0
Reflector 1	1002.7	1002.3	1002.1	1002.6	1002.8	1002.9	1002.8	1003.0
Reflector 2	1301.4	1308.9	1315.3	1334.8	1354.6	1373.9	1383.8	1392.3
Reflector 3	1569.7	1586.6	1603.1	1613.1	1617.9	1612.7	1609.4	1603.9
Reflector 4	1998.0	1998.5	1998.9	1998.5	1998.4	1998.5	1998.3	1998.0

While the errors in depth due to the slightly different offset are small, increasing from left to right, a more direct comparison of the recovered reflector depths and the model values has been assembled in Table 4. The recovered reflector depths seen in Table 3 have been interpolated using the cubic spline definition to the same offset values as the model.

The range of errors in the recovered reflector depths seen in Table 4 is -2.3–3.1 ft. The rms error of the recovered reflector depths is 1.4 ft. These errors basically confirm the theoretical predictions of Bube and Langan (1995) for a 600 ft tomographic inversion. This resolution of reflector depth seems quite remarkable considering the 10.0 ft constant slowness cell parameterization. The primary source of errors are reflectors 2 and 3. The calculated location of reflector 2 is uniformly shallow while reflector 3 is uniformly deep. This is a result of the direction of the reflection raypaths with respect to velocity contrast.

TABLE 4. Resampled* reflector depth inversion results and synthetic model #1 reflector depths

Offset (ft)	0.0	94.29	188.57	282.86	377.14	471.43	565.71	660.0
Ref.1 model	1003.0	1003.0	1003.0	1003.0	1003.0	1003.0	1003.0	1003.0
Ref.1 result*	1002.7	1002.3	1002.1	1002.6	1002.7	1002.9	1002.8	1002.9
Ref.2 model	1302.0	1310.0	1315.0	1335.0	1355.0	1375.0	1385.0	1392.0
Ref.2 result*	1301.4	1308.8	1315.0	1333.8	1353.4	1372.7	1383.2	1391.2
Ref.3 model	1569.0	1584.0	1600.0	1610.0	1615.0	1610.0	1607.0	1604.0
Ref.3 result*	1569.7	1586.3	1602.7	1612.7	1617.9	1613.1	1609.7	1604.7
Ref.4 model	1998.0	1998.0	1998.0	1998.0	1998.0	1998.0	1998.0	1998.0
Ref.4 result*	1998.0	1998.5	1998.9	1998.5	1998.4	1998.5	1998.3	1998.0

*The reflector inversion results have been interpolated using a cubic spline interpolation to obtain reflector depths for the same reflector x offsets as the original model so that a direct comparison can be made.

Reflection traveltimes obtained from reflector 3 are for upgoing raypaths. The ability of the inversion routine to locate exactly a reflector defined by a sharp interface is related to the ability of the inversion to define the interface itself. Since the velocity gradient in the

vertical direction is somewhat smooth the reflector must be shifted slightly to compensate for the gradient. In the case of reflector 3, a low velocity zone overlies a high velocity zone and the raypaths travel primarily through low velocities. The smooth gradient causes the raypaths to travel through velocities which are a little too high near the reflector. This results in a calculated traveltime which is too low if the reflector is properly located. To compensate for this the reflector is shifted down slightly to lengthen the raypaths and increase the traveltimes. The same reflector would be shifted up slightly if the model consisted of a high velocity zone overlying a low velocity zone. This same reasoning applies to reflector 2 except that the direction of the correction is opposite since the location of this reflector is calculated using downgoing rays.

SYNTHETIC STUDY #2

I designed the second example to test the ability of the direct and reflected arrival traveltime inversion to recover reflector geometries when the reflectors are discontinuous. The model used to generate the direct and reflected arrival traveltimes is shown in Figure 3. This model includes 5 dipping layers that have been thrown offset by a steeply-dipping normal fault. I have also included a low velocity layer near the bottom of the model with a velocity contrast across the fault. This situation is designed to mimic a possible field experiment where the target exists near the bottom of the survey. This is a situation where traditional direct arrival tomography has poor lateral resolution.

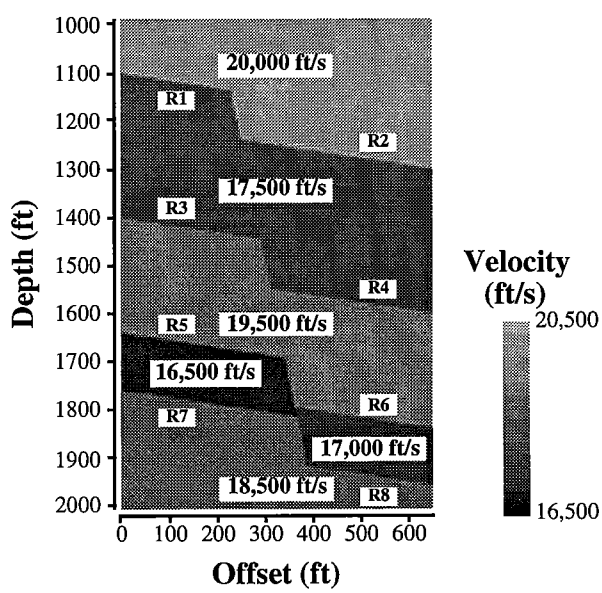

Figure 3: Velocity model used to generate traveltime data for synthetic study #2. Reflectors are numbered from top to bottom. Discontinuous reflectors are defined by the individual segments. Reflector depths can be found in Table 5.

The dimensions of the model shown in Fig. 3 are identical to those of the first synthetic model (Fig. 1) except that the new model is 650.0 ft across rather than 660.0 ft. The interfaces are linear, except at the fault point, and dip uniformly at 8.75° from the receiver well to the source well. Each reflector can be completely described by the point at which it in-

tersect a well and the point it intersects the fault. The broken reflectors have been numbered separately to maintain a consistency with the inversion routine which solves for the broken pieces of a discontinuous reflector as separate individual reflectors. The geometries of the reflectors are given in Table 5.

TABLE 5. Synthetic model #2 reflector data

	Receiver Well intersection depth (ft)	Fault Plane intersection point x,z (ft)	Source Well intersection depth (ft)
Reflector 1	1100.0	227.0, 1134.9	null
Reflector 2	null	247.6, 1238.1	1300.0
Reflector 3	1400.0	288.9, 1444.4	null
Reflector 4	null	309.5, 1547.6	1600.0
Reflector 5	1640.0	338.4, 1692.1	null
Reflector 6	null	359.0, 1795.2	1840.0
Reflector 7	1760.0	363.2, 1815.9	null
Reflector 8	null	383.8, 1919.0	1960.0

Synthetic Study #2: Acquisition Geometry and Data Specifications

The source and receiver acquisition geometry of synthetic survey #2 is almost identical to that of survey #1 except that the source-receiver offset is 650.0 ft. There are 201x201 sources and receivers spaced evenly every 5.0 ft from 1000.0–2000.0 ft. As with survey #1, traveltimes were initially calculated for all source-receiver-reflector combinations and then edited to provide a more realistic traveltime data set. Direct arrival traveltimes have been prepared in a slightly different manner in this example. All near offset direct arrival traveltimes have been kept for the inversion. Far offset traveltimes are limited to ±50.0°, about 775 ft in offset. Reflected traveltime arrivals have been edited in much the same way as in the Study #1. The reflection data for each reflector are edited to include traveltimes of either upgoing or downgoing events. The traveltimes are further edited to provide a reasonable range of incidence angles. Table 6 provides information on the traveltimes used for the various reflectors.

TABLE 6. Specifications of Example 2 reflection traveltime data

	Direction	# Traveltimes
Reflector 1	downgoing	1495
Reflector 2	downgoing	6976
Reflector 3	downgoing	3841
Reflector 4	upgoing	4091
Reflector 5	upgoing	5290
Reflector 6	upgoing	5060
Reflector 7	upgoing	6471
Reflector 8	upgoing	2811

Synthetic Study #2: Inversion and Results

I ran a direct and reflected arrival inversion on synthetic data set #2 starting with a homogeneous model with 10.0 ft cells and flat reflectors each defined by 34 nodes. The initial reflector depths for reflectors 1-8 respectively were: 1090.0, 1290.0, 1395.0, 1610.0, 1755.0, 1850.0, 1870.0, and 1970.0 ft. Since part of the information desired from the inversion is an estimate of the reflector extent the reflectors were parameterized using a higher number of nodes. From the final result, the segments of each reflector that are subject to reflections are interpreted to define the reflector extent.

The initial values of the smoothing penalties weights in this inversion differ slightly from the values used in Study #1. Like Study #1, the initial weight of the horizontal smoothing penalty equals the weight of the traveltime data and the vertical smoothing penalty weight is 1/4th of the horizontal weight the entire inversion. But, in this inversion, the initial reflector second derivative smoothing penalty weight *equals* the horizontal weight. The reflector smoothing was initialized at a higher value in this example to help stabilize the larger number of nodes used to define each reflector. Another difference in this inversion is that *all* smoothing penalty terms were relaxed an order of magnitude every 4 continuation steps.

The ideal, or "best", answer is the result of continuation step 10. Traveltime residuals are ~108μs rms for the 33,884 reflected rays and ~120μs rms for the 37,873 direct arrival rays. Note in this example that the direct arrival traveltime residuals are slightly higher than the reflected arrival residuals. This result is due to an increased ratio of reflected traveltimes to direct arrival traveltimes and the inclusion of near-offset direct-arrival traveltimes which themselves have higher residuals.

The final tomogram is shown in Figure 4. Note that the resolution is somewhat low and similar to the result of Study #1. Although the resolution is low the existence of a fault can be seen clearly, especially at the bottom of the image. The different velocities of the thin layer near the bottom can also be identified in the image.

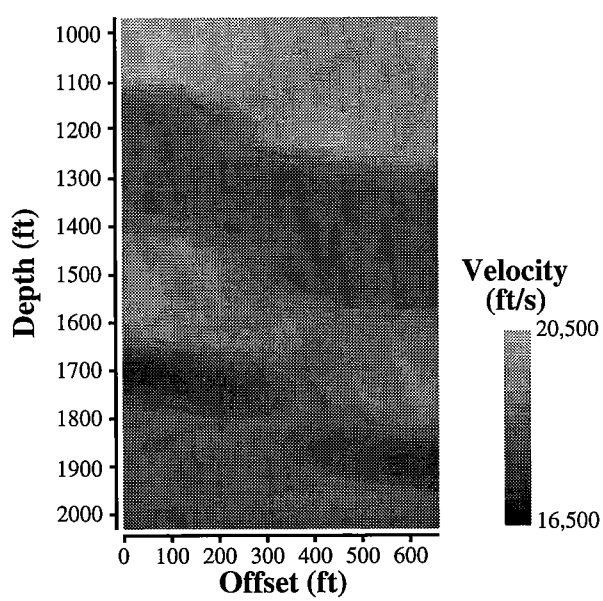

Figure 4: The resulting velocity tomogram obtained after 10 continuation steps of a combined direct and reflected arrival traveltime inversion. This result should be compared to the velocity model shown in Fig. 3 which was used to generate the traveltime data.

The reflector depth results obtained in this example are interpreted in a slightly different manner than in Study #1 although the inversions are run in much the same way. The lateral extent of the reflectors is never known *a priori* so each reflector is initially assumed to extend all the way across the model. After the inversion is complete an estimate of the lateral extent of the reflectors can be recovered based on the raypath coverage of each reflector segment. By using 34 nodes to describe the reflectors across the 660.0 ft model the distance between nodes is 20.0 ft. The coverage is maintained by keeping track of the number of non-zero derivatives of each reflector depth parameter. In this inversion the average number of non-zero derivatives for all reflector parameters is 490.6. I have set the cutoff for the number of non-zero parameters to qualify a segment as being "covered" as 6. This cutoff value affects only 6 reflector segments. To aid in the visualization of the reflector recovery I have plotted the "covered" reflector solutions in Figure 5 as an overlay to the original model.

Figure 5 shows that direct and reflected arrival traveltime inversion locates the reflectors fairly well in depth and also in extent. The largest errors in depth appear in reflector 1, 2, 7, and 8. A similar mispositioning phenomena to that seen in Study #1 can be seen. Reflectors 1 and 2, determined by downgoing reflections, with a high velocity layer overlying a low velocity layer, are too shallow just like reflector 2 in Study #1. Reflectors 7 and 8, determined by upgoing reflectors, with a low velocity layer overlying a high velocity layer, are too deep just like reflector 3 of the first study. The magnitude of the errors is a bit larger this time though.

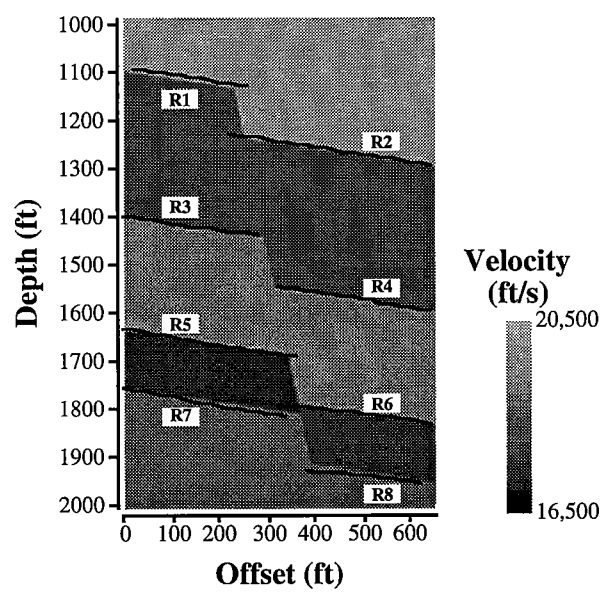

Figure 5: The reflector depth locations obtained from the traveltime inversion plotted on top of the original velocity model used to generate the synthetic data. The reflectors are actually defined across the entire velocity image but only reflector parameters with a significant number of non-zero depth derivatives have been plotted.

To provide a graphic display of the reflector depth errors they have been plotted in Figure 6. The extent of the reflector depth errors is from about -10–12 ft, a bit larger than found in the previous example. Note that largest errors occur in reflectors near the top and bottom

of the image. There are several possible explanations to be investigated at a later date. First, the top and bottom layers are covered by relatively few direct arrival raypaths. This may make it more difficult to calculate a sharp velocity gradient at these interfaces. Second, this inversion ran only 10 continuation steps before it became unstable. This means the smoothing penalty terms are still relatively strong compared to Study #1, preventing sharp velocity gradients. Finally, the forward modeler used to calculate the direct arrival traveltimes is more prone to errors near sharp, nearly-horizontal interfaces. It may be that there are significant errors in these traveltimes preventing the inversion from correctly calculating the sharp interfaces.

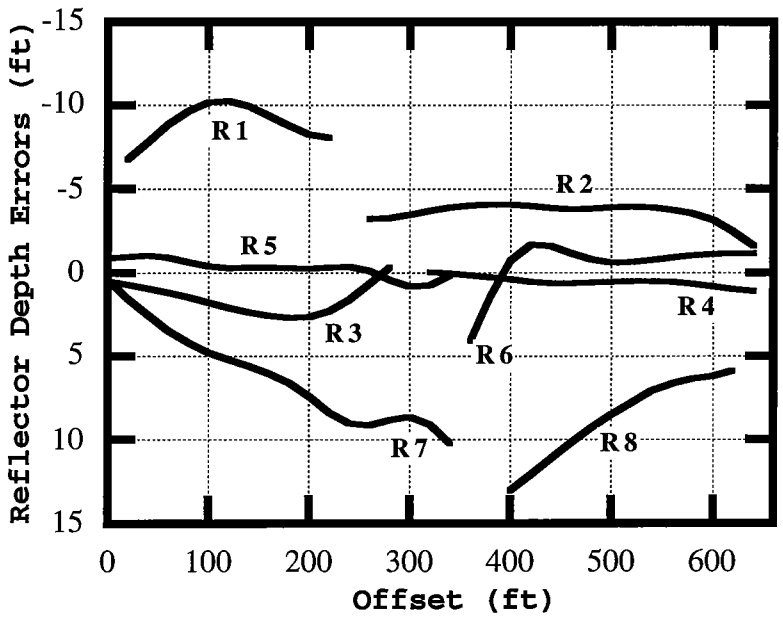

Figure 6: The difference between the reflector depths obtained from the traveltime inversion and the actual model depths shown if Fig. 5. Note that the largest errors are in the reflector depths near the top and bottom of the model.

COMBINED STUDY #3

Combined study #3 consists of a field data traveltime inversion and a synthetic data traveltime inversion. The field data set is from the McElroy Reservoir Geosciences Project (MRGP) (Harris et al., 1995). Reflected and direct arrival *S*-wave traveltimes have been collected from the near offset (~188 ft) survey between wells McElroy 1202 and McElroy 1068. The data used are actually a subset of the entire data set to keep the traveltime inversion problem within the capabilities of the computer hardware.

The synthetic part of this study is designed to parallel the field inversion in processing, source/receiver acquisition geometry, and model characteristics. The goal is to obtain an estimate of the resolution of the field survey by studying the results of an inversion on a synthetic data set. The synthetic data are calculated using a velocity model containing many of the features of the field geology. Figure 7 shows the model used to create the synthetic data. This model is based on a smoothed version of the receiver well (McElroy 1202) *S*-

wave sonic log, seen on either side of the model in Fig. 7, and information on the reflector geometries at the McElroy site.

The geometries of the reflectors at the McElroy site are based on an interpretation of the traveltime picks and the crosswell reflection image (Lazaratos et al., 1995). To interpret reflector geometries from the field data set requires reflection traveltimes for reflectors R1–R9, seen in Fig. 7, and the direct arrival traveltimes. The intersection of the direct and reflected arrivals provides an estimate of the intersection of the reflecting horizons and the wells. An analysis of the crosswell reflection image shows that although the picked reflectors are dipping to various degrees that they are basically linear. The reflectors used in the design of the synthetic model, shown in Fig. 7, reflect these observations.

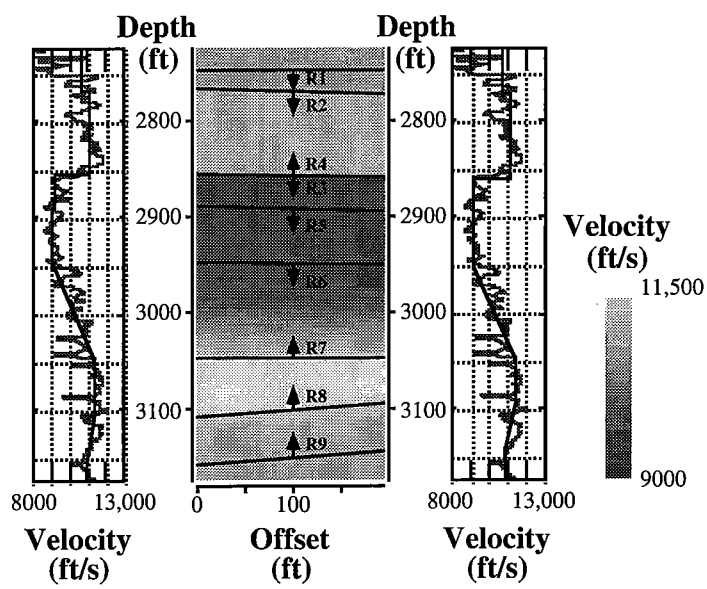

Figure 7: The synthetic model used in Study #3. The simple velocity profile is an approximation of the receiver well *S*-wave sonic log. The velocity profile on the right side is perturbed to reflect the change in reflector depths across the model. The location and nature of these reflectors is believed to reflect the geology at the McElroy site. Arrows on the reflectors indicate the nature (upgoing or downgoing) of the reflected arrival traveltime picks obtained from the field data set. The synthetic traveltime picks were edited to include picks for the same source-receiver-reflector combinations as the field data set.

Table 7 provides details of the reflector geometries for the synthetic model. Since the reflectors are linear they can be completely defined by their intersection points with the wells. The primary difference between the setup of the field and synthetic survey is that the well deviations of the field survey were not used to create the synthetic model. In the synthetic model the wells are assumed to be vertical with an offset of 195.0 ft. Note that reflectors 3 and 4 are identical in location. They are defined as separate reflectors to remain consistent with the field data inversion.

In field data, traveltimes may be picked for an event that can be seen in both upgoing and downgoing data sets. For a series of closely spaced reflectors the shape of the upgoing and downgoing reflections may differ by more than a phase reversal. This potential difference in phase results in traveltime picks that correspond to slightly different depths in the

correct velocity field. In other words, the peak of an upgoing reflection may not exactly correspond in depth to the trough of a downgoing reflection when mapped. Another similar potential problem can occur even if a strong reflection is isolated, meaning that upgoing and downgoing reflections *should* differ by a simple phase reversal. In this case the separate processing of the upgoing and downgoing data sets may introduce phase shifts in the data which mimic the interference error. Rather than trying to monitor and correct this problem the upgoing and downgoing events are inverted as separate reflectors.

TABLE 7. Synthetic model #3 well intersection depths

	Receiver Well intersection depth (ft)	Source Well intersection depth (ft)
Reflector 1	2746.0	2748.5
Reflector 2	2767.5	2772.5
Reflector 3	2855.0	2860.0
Reflector 4	2855.0	2860.0
Reflector 5	2890.0	2895.0
Reflector 6	2947.5	2952.5
Reflector 7	3048.5	3048.5
Reflector 8	3107.0	3092.0
Reflector 9	3157.5	3142.5

Combined Study #3: Acquisition Geometry and Data Specifications

As previously mentioned, the synthetic data are edited to have non-zero traveltimes for the same source-receiver-reflector combinations as the field data set. So the primary difference in the data sets should be in the well configurations, the field data set having deviated wells and the synthetic data set having vertical wells. The surveys consist of 162 sources from 2745.0–3147.5 ft by 167 receivers located from 2745.0–3160.0 ft, every 2.5 ft.

S-waves are not produced by the piezoelectric source at near offsets and the minimum offset for which direct arrival traveltimes are available is about 55 ft. Direct arrival traveltimes have been collected for all larger offsets. Reflection traveltimes were picked manually from the field data set from wavefield data in the CDP domain. Prior to reflection traveltime picking, the data are processed as 2 separate data sets to enhance the *S*-wave reflections from upgoing and downgoing events. Table 8 provides information about the reflection traveltime picks.

TABLE 8. Field and synthetic reflection traveltime coverage

	Direction	# Traveltimes
Reflector 1	downgoing	4392
Reflector 2	downgoing	4275
Reflector 3	downgoing	4940
Reflector 4	upgoing	783

TABLE 8. Field and synthetic reflection traveltime coverage

	Direction	# Traveltimes
Reflector 5	downgoing	2664
Reflector 6	downgoing	3872
Reflector 7	upgoing	6399
Reflector 8	upgoing	4264
Reflector 9	upgoing	4203

Combined Study #3: Inversion

The inversions of both synthetic and field data were run using identical processing parameters. Direct arrival traveltimes were limited to a ±65.0° aperture, equivalent to approximately 420 ft in offset. At the beginning of the inversion the weights of the second derivative reflector smoothing penalty and the horizontal smoothing penalty were set equal the weight of the traveltime data while the vertical smoothing weight was 1/8th the weight of the horizontal smoothing. The penalty weights were relaxed at a rate of one order of magnitude every 4 continuation steps.

The initial slowness model used in both inversions is homogeneous and equal the average slowness of the direct arrival traveltimes (of the field data set). The cell size of the slowness model is 5.0 ft by 5.0 ft. The reflectors are defined with 21 nodes each, equal to 10.0 ft between nodes. Like Study 1 and Study 2, the inversions were started with flat reflectors. The starting depths for reflectors 1-9 respectively are: 2750.0, 2770.0, 2860.0, 2855.0, 2890.0, 2950.0, 3050.0, 3100.0, and 3150.0.

Combined Study #3: Synthetic Data Results

The results of the 12th continuation step of the synthetic data inversion are optimal for a direct comparison with the field data inversion. Traveltime residuals are ~24μs rms for the 35,237 reflected rays and ~18μs rms for the 20,163 direct arrival rays. These residuals are very near the resolution of the code used to calculate the traveltimes of the raypaths. The velocity tomogram, shown in Figure 8 shows the simple features of the velocity model with few artifacts.

The calculated reflector depths have a range of errors of -1.27–0.73 ft and an rms depth error of 0.54 ft, ~6.5 *inches* . This result confirms the theoretical estimate of Bube and Langan for a ~180 ft crosswell profile. Table 9 provides an abbreviated listing of the inversion results along with the model parameters. Every other parameter in offset (11 out of 21) is shown in this listing. One observation that can be made from data in Table 9 is that the largest depth errors occur in reflectors 3 and 4. These reflectors occur at the interface of two zones with a high velocity contrast. The slow layer lies beneath the fast layer.

The errors in reflectors 3 and 4 are exactly of the type that was previously discussed in Studies 1 and 2. Reflector 3, determined by downgoing reflections in the slower material, is slightly shallow over its entire length. Reflector 4, determined by upgoing reflections in the faster layer, is *also* shallow. This is the situation predicted but not observed in Studies 1 and 2. Due to the velocity gradient in the vicinity of the correct reflector location, the upgoing reflected ray travels through slow material near the interface. The increase in travel-

time caused by the slow material forces the reflector up, so that the raypath is shortened and the traveltime is compensated.

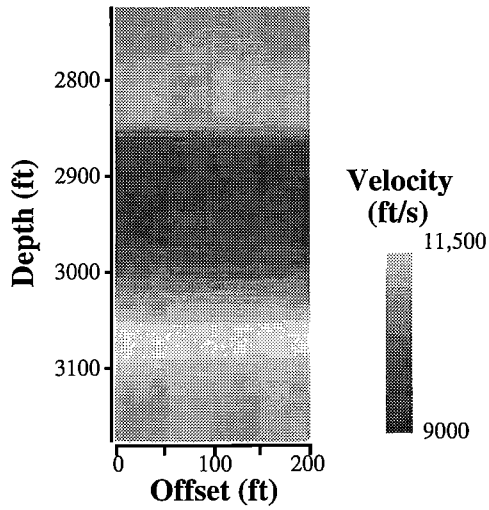

Figure 8: The tomogram result of the 12th continuation step of the synthetic data inversion. The rms error of the 55,400 direct and reflected traveltimes used in this inversion is 20.3 μs. This tomogram can be compared with the model used to generate the synthetic data shown in Fig. 7.

TABLE 9. Synthetic model #3 and synthetic inversion reflector depths

Offset (ft)	0.0	20.0	40.0	60.0	80.0	100.0	120.0	140.0	160.0	180.0	200.0
R1 model	2746.0	2746.3	2746.5	2746.8	2747.0	2747.3	2747.5	2747.8	2748.1	2748.3	2748.6
R1 result	2745.9	2746.0	2746.1	2746.3	2746.5	2746.9	2747.2	2747.6	2747.9	2748.2	2748.5
R2 model	2767.5	2768.0	2768.5	2769.0	2769.6	2770.1	2770.6	2771.1	2771.6	2772.1	2772.6
R2 result	2767.6	2768.1	2768.6	2769.1	2769.6	2770.1	2770.7	2771.3	2771.9	2772.4	2772.7
R3 model	2855.0	2855.5	2856.0	2856.5	2857.1	2857.6	2858.1	2858.6	2859.1	2859.6	2860.1
R3 result	2854.5	2854.7	2855.1	2855.5	2855.9	2856.3	2856.8	2857.5	2858.1	2858.8	2859.5
R4 model	2855.0	2855.5	2856.0	2856.5	2857.1	2857.6	2858.1	2858.6	2859.1	2859.6	2860.1
R4 result	2854.2	2854.7	2855.1	2855.6	2856.1	2856.5	2857.0	2857.6	2858.1	2858.7	2859.3
R5 model	2890.0	2890.5	2891.0	2891.5	2892.1	2892.6	2893.1	2893.6	2894.1	2894.6	2895.1
R5 result	2889.9	2890.5	2891.1	2891.7	2892.3	2892.7	2893.2	2893.6	2894.1	2894.5	2894.9
R6 model	2947.5	2948.0	2948.5	2949.0	2949.6	2950.1	2950.6	2951.1	2951.6	2952.1	2952.6
R6 result	2947.5	2948.0	2948.5	2949.0	2949.4	2949.9	2950.5	2951.0	2951.5	2952.0	2952.5
R7 model	3048.0	3048.0	3048.0	3048.0	3048.0	3048.0	3048.0	3048.0	3048.0	3048.0	3048.0
R7 result	3048.5	3048.5	3048.5	3048.5	3048.5	3048.4	3048.4	3048.5	3048.5	3048.5	3048.7
R8 model	3107.0	3105.5	3103.9	3102.4	3100.8	3099.3	3097.8	3096.2	3094.7	3093.2	3091.6
R8 result	3107.0	3105.5	3103.9	3102.4	3100.9	3099.3	3097.7	3096.2	3094.6	3093.1	3091.7
R9 model	3157.0	3155.5	3153.9	3152.4	3150.8	3149.3	3147.8	3146.2	3144.7	3143.2	3141.6
R9 result	3157.6	3156.1	3154.6	3153.0	3151.4	3149.8	3148.3	3146.7	3145.2	3143.7	3142.3

COMBINED STUDY #3: FIELD DATA RESULTS

The best answer in the tomographic inversion of the McElroy *S*-wave field data is the result of continuation step 12. Traveltime residuals are ~108μs rms for the 35,680 reflected rays and ~65μs rms for the 20,114 direct arrival rays. The combined rms error is ~95μs. The velocity tomogram from continuation step 12 is shown in Figure 9. The tomogram shows quite a bit more lateral variation than seen in the synthetic study. In the low velocity zone in the middle of the image the slower regions are concentrated towards the edge of the model.

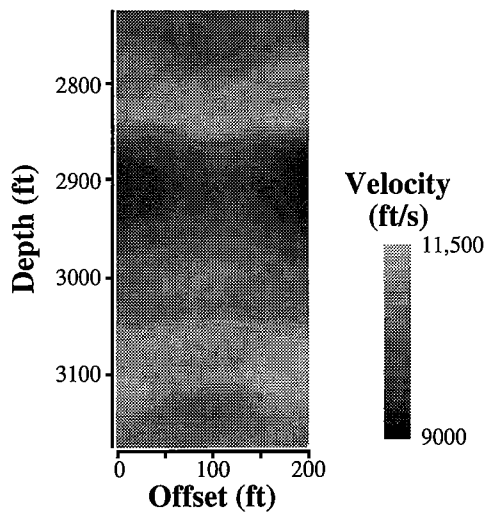

Figure 9: The *S*-wave velocity tomogram from the McElroy field data set created using direct and reflected traveltime arrivals. This tomogram is the result of the 12th continuation step. The overall traveltime residual is ~95 μs rms for the 55,794 traveltimes used in this inversion.

The reflector depths obtained in the inversion are plotted over an *S*-wave crosswell reflection image in Figure 10. The calculated reflectors match the structure seen in the reflection image in a general way but several reflectors are distinctly non-linear. In particular, reflectors 1 and 7 drift a fair amount compared to the image. Several other reflectors are a bit more linear. Reflectors 3 and 4, located at about 2850 ft, almost exactly overlay each other and follow the moveout of the reflection image quite closely.

Compared to the almost perfect recovery of the reflector depths in the synthetic example the mild disagreement between the calculated reflector geometries and the reflection structure seen in the crosswell reflection image (Fig. 10) is interesting. This disagreement suggests that some other parameter may be affecting the inversion. There are several different possibilities to be studied: errors in the traveltime picking, well deviation errors, timing errors, or velocity anisotropy.

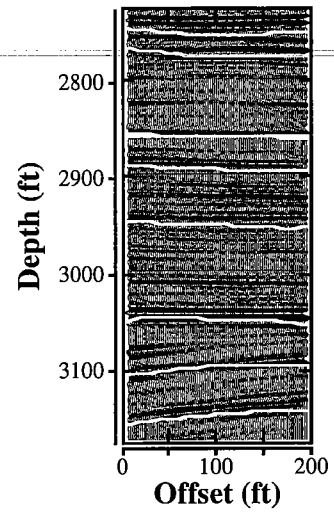

Figure 10: The reflector solutions of the direct and reflected arrival traveltime inversion plotted over the *S*-wave crosswell reflection image (Lazaratos, 1995).

CONCLUSIONS

The results of the combined direct and reflected arrival traveltimes inversions shown in this paper support the theoretical predictions that reflector locations are well resolved in crosswell data. In a synthetic example designed around the McElroy 188 ft. offset survey, reflector depths were recovered with an rms error of 6.5 *inches* . This survey and other, larger offset surveys, achieved a resolution in reflector depths very close to the values predicted by theoretical studies done by Bube and Langan (1995).

The field data example, an *S*-wave data set from the McElroy Reservoir Geosciences Project, produced results that were also quite promising. While the reflector geometries calculated using the traveltime inversion had some differences compared to the crosswell reflection image created from the same data, at least one major feature was recovered quite well. The unconformity, located at ~3050 ft, can be seen quite easily in the calculated reflector depths.

The success of these inversions opens a wide range of related areas to study. The next step is to determine the effectiveness of using combined direct and reflected arrival traveltime tomography as a velocity analysis tool for reflection imaging. Currently, obtaining an effective velocity model and reflector geometries for VSP-CDP mapping is the most labor intensive of the imaging steps. Planned future research is to develop a mapping algorithm that uses the velocity image and reflector geometries provided by the traveltime inversion to map the wavefield data directly.

ACKNOWLEDGEMENTS

I would like to thank Ken Bube and Robert Langan for providing me with their traveltime inversion code and helpful guidance. I would also like to thank Jesse Costa for his invaluable assistance in providing me insights to the inversion process. I would finally like to thank Jerry Harris and the sponsors of the STP consortia for providing support for this work

REFERENCES

Bishop, T. N., Bube, K. P., Cutler, R. T., Langan, R. T., Love, P. L., Resnick, J. R., Shuey, R. T., Spindler, D. A., and Wyld, H. W., 1985, Tomographic determination of velocity and depth in laterally varying media: Geophysics, **50**, 903–923.

Bube, B. P., Langan, R. T., and Resnick, J. R., 1989, Unique determination of reflector depths in seismic reflection tomography: 59th Ann. Internat. Mtg., Soc. Expl. Geophys., Expanded Abstracts, 918–921.

Bube, B. P., and Langan, R. T., 1995, Resolution of crosswell tomography with transmitted and reflected traveltimes: STP-**6**, Paper I

Calnan, C., and Schuster, G. T., 1989, Reflection + Transmission Crosswell Tomography: 59th Ann. Internat. Mtg., Soc. Expl. Geophys., Expanded Abstracts, 908–911.

Harris, J. M., Nolen-Hoeksema, R. C., Rector, J. W., Lazaratos, S. K., and Van Schaack, M. A., 1995, High-resolution crosswell imaging of a west Texas carbonate reservoir: Part 1—Project summary and interpretation: Geophysics, **60**, 667–681.

Ivansson, S., 1986, Some remarks concerning seismic reflection tomography and velocity analysis: Geophys. J. R. Astr. Soc., **87**, 539–557.

Lazaratos, S. K., 1993, Cross-well reflection imaging: Ph.D. thesis, Stanford University.

Lazaratos, S. K., Harris, J. M., Rector, J. W., and Van Schaack, M. A., 1995, High-resolution crosswell imaging of a west Texas carbonate reservoir: Part 4—Reflection imaging: Geophysics, **60**, 702–711.

Stork, C., 1988, Ray trace tomographic velocity analysis of surface seismic reflection data: Ph.D. Thesis, Calif. Inst. of Technology.